Modeling and Simulation of Underwater Textile-Based Soft Robotic Gripper

Amneh Nasir
Amneh.Nasir@tecnico.ulisboa.pt

Instituto Superior Técnico, Lisboa, Portugal

November 2023

Abstract

This thesis introduces the development of an underwater textile-based soft robotic gripper, focusing on the delicate handling of marine samples. Traditional methods, such as the use of human divers or remotely operated vehicles (ROVs) with rigid manipulators, are often inadequate due to their lack of precision and adaptability for handling sensitive marine life. To address these challenges, the research builds upon the Textile Robotic Hand (TRH) from Technische Universität München, integrating air-pump actuation with curvature and pressure sensors. The mechanics of the robot are meticulously modeled to meet the unique requirements of underwater manipulation, and multiple simulation platforms are employed to evaluate its motion. In addition, the TRH components are assessed and modification are proposed to ensure optimal functionality in underwater environments, including the transition from the initial pneumatic actuation system to one more suitable for aquatic conditions. The proposed soft robotic manipulator marks a significant advancement in underwater robotics and offers a more effective solution for marine sampling.
Keywords: Underwater Manipulators; Textile Robotics; SOFA Framework ; Mechanical Modeling.

1. Introduction

The exploration of the ocean's depths has long captivated human curiosity, with a growing emphasis on understanding the intricate ecosystems beneath the waves. Sampling plays a pivotal role in marine research, aiding in the comprehension of diverse marine life within these ecosystems. However, traditional sampling methods, involving human divers, lack the adaptability necessary for handling delicate marine species, as divers cannot reach great depths at which samples can reside. And Remotely Operated Vehicle (ROV)s equipped with rigid manipulators, often lack the precision necessary for handling delicate marine species,due to their rigid design for industrial applications making them possibly harmful to the specimens. This inadequacy poses a risk of harm to sensitive delicate marine life, such as millennia-old deep-sea corals and long-living giant clams, which are integral to marine biodiversity.

In response to these challenges, the field of soft robotics emerges as a promising solution. Soft robotic manipulators, characterized by their flexibility and compliance, offer an innovative approach to handle delicate marine samples safely and efficiently. This thesis focuses on the adaptation and optimization of a Textile Robotic Hand (TRH), originally developed by Technische Universität München [1], for underwater applications. The TRH, utilizing air-pump actuation combined with curvature and pressure sensors, is adapted for underwater use, addressing the unique challenges posed by the aquatic environment, such as water pressure and drag.

The methodological approach of this study involves the use of advanced simulation platforms, including SOFA, Abaqus, and SolidWorks. These tools are employed to predict and analyze the behavior of the TRH. The objective is to identify the most suitable simulation environment that accurately represents the manipulator's performance in underwater conditions.

Figure 1: Various poses of the TRH alongside a wearable fabric glove [2]

The significance of this research extends be-

yond marine biology. By adapting and optimizing existing soft robotic systems, this study aims to enhance their adaptability and versatility in challenging environments.

Section 2 will introduces the most important references for this thesis. Section 3 details the methods used to Model the TRH while accounting for the underwater affects. Section3.3 discusses the different methodologies used for the simulation. Section 4 depicts the results, and Section 5 presents the conclusions and future work.

2. Background

The journey of soft robotics began in the 1950s with McKibben's pneumatic artificial muscles [3] and has since expanded into various fields, including underwater exploration [4]. Innovations such as the elephant trunk robot [5] and the octopus-inspired robot [6] paved the way for modern developments like textile robotic hands [1] and soft robotic grippers [7], demonstrating their adaptability in challenging marine environments [8].

Soft robotic manipulators, crafted from materials like elastomers and textiles, offer unparalleled flexibility and safe interaction capabilities. Key developments in this area include Rus et al.'s soft gripper [9] and Polygerinos et al.'s pneumatic manipulator [10], with recent innovations focusing on enhancing dexterity and integrating sensors for improved functionality [11, 12]. The intersection of robotics and textiles has led to the creation of versatile fabric-based robots with applications in healthcare and industrial automation. Early examples include a knitted robotic arm [13] and a starfish-inspired gripper [14], with recent advancements involving 3D printing techniques and the integration of sensors for enhanced control [15, 16].

Material selection is crucial in the design and functionality of soft robots, with each material's mechanical properties dictating its behavior under various conditions as per table 1 . For instance, silicone elastomers like polydimethylsiloxane (PDMS) are favored for their bio-compatibility and tunable mechanical properties [17]. Hydrogels, known for their volume-changing response to environmental stimuli, are explored for their potential in soft robotics [18]. Thermoplastic Polyurethane (TPU), notable for its balance of flexibility and strength, is particularly useful in underwater applications due to its durability in complex environments [19]. When combined with materials like High Strength Polyester Ribbon (HSPR), TPU's properties are further enhanced, making it ideal for challenging conditions [20].

Advanced simulation tools, such as Finite Element Method (FEM), Abaqus, and SOFA, are instrumental in soft robotics design. These tools model complex behaviors and interactions under various conditions, optimizing design for specific tasks [23, 24]. SOFA, in particular, offers a versatile simulation platform for soft robotics, supporting diverse modeling methodologies and real-time feedback, crucial for iterative design [24].

Material	Young's Modulus (MPa)	Poisson's Ratio	Density (g/cm^3)	Tensile Strength (MPa)
PDMS	0.5 - 3 [21]	0.49	0.97 - 1.03	2.5 - 4.5
Hydrogel	0.001 - 1 [22]	0.45 - 0.5	1.0 - 1.2	0.1 - 1
TPU	1 - 5	0.4 - 0.5	1.1 - 1.2	25 - 50
HSPR	6 - 12 [20]	0.35 - 0.4	1.38	80 - 120

Table 1: Mechanical properties of common soft robotic materials.

In marine environments, soft robots excel in tasks like deep-sea exploration and marine conservation. Pioneering research in this field includes Galloway's work on coral sampling and Katzschmann's autonomous robotic fish, as illustrated in table 2.

Reference	Material	Depth	Actuation
Galloway et al. [25]	Soft elastomers	Deep reefs	Fiber-reinforced
Stuart et al. [26]	Advanced polymers	100m	Bellows-style
Vogt et al. [27]	3D printed elastomers	300m	Bellows
Marchese et al. [28]	Silicone elastomers	200m	Pneumatic
Katzschmann et al. [29]	Soft silicone	50m	Pneumatic

Table 2: Overview of key studies on soft underwater manipulators.

Advancements in underwater sensors, such as pressure and curvature sensors, have significantly enhanced the capabilities of soft manipulators in challenging marine environments [30, 31, 32, 33]. Looking forward, the field of soft underwater robotics, with its adaptability and gentle interaction, is poised to transform marine exploration and research. Future developments should focus on enhancing durability and integrating AI for autonomous operations [34, 30, 31].

Finally, understanding the complex interplay of hydrodynamic forces is crucial for the design and operation of efficient manipulators. Drawing from Fossen's seminal work on marine craft hydrodynamics [35], this research delves into the intricacies of hydrostatics, added mass, and hydrodynamic damping and coefficients. Fossen's comprehensive analysis provides a foundational understanding of the forces at play in the underwater environment, such as buoyancy, drag, and lift, which are pivotal in determining the stability and maneuverability of underwater systems. These insights are instrumental in developing robust models for underwater manipulators, ensuring their op-

timal performance in the dynamic and often unpredictable marine environment.

3. Modeling

3.1. Torque Model in Underwater Environments

This subsection presents a comprehensive torque model for underwater actuators, incorporating various factors to the flexion-extension mechanics based on [2]. Drawing from Fossen's comprehensive insights on marine craft hydrodynamics[35], such as hydrostatic pressure, added mass, friction, and water resistance.

The main model considered an actuator comprised of two interacting segments. The contact force F between the two pressurized segments depends on the internal pressure P and was calculated as follows:

$$F = \pi l P \left(\frac{r^2 - a^2}{2r} \right). \tag{1}$$

Where l is the length, r is the radius, and a is the distance between the center of the segment and the contact point. This force is responsible for the actuator's bending motion. The pressure inside the actuator segments works against the contact area to produce a torque τ which is applied at the housing fabric:

$$\tau = \pi l P \left(\frac{r^2 - a^2}{2} \right). \tag{2}$$

The contact angle β is the angle between the normal to the contact area between the two segments of the flexion actuator and the line connecting the centers of the two segments. As the actuator bends, the contact angle changes, which in turn affects the contact force and torque. This angle is connected to the actuator angle θ through the equations:

$$\beta = \arcsin\left(a/(r + r_c)\right) \tag{3}$$

$$a = \left(r + \frac{nw}{2\pi - \theta} \right) \sin\left(\frac{2\pi - \theta}{2n} \right). \tag{4}$$

The contact angle is important because it determines the direction of the contact force. This change in the direction of the contact force is what causes the actuator to bend. In this equation, n represents the number of segments, and w stands for the width of a single segment, which is demonstrated in figure 2.

Now to the paper consideration of an extension actuator, which will re-extend the curved part after flexsion. The actuator's performance can be described in terms of the torque τ it can generate. The torque depends on the actuator's geometric parameters, such as its radius r and length l, the deflection angle ρ, and the internal air pressure P.

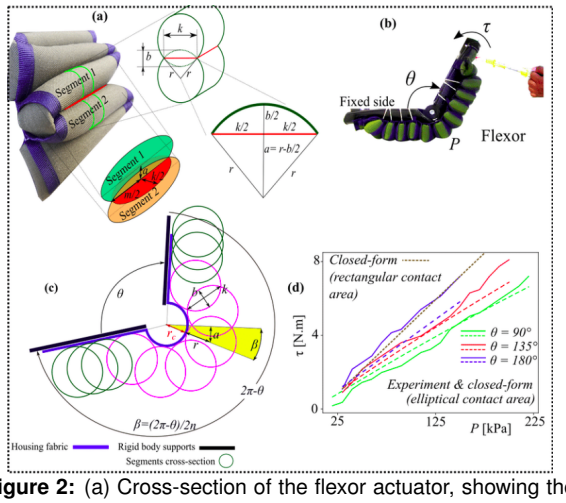

Figure 2: (a) Cross-section of the flexor actuator, showing the elliptical contact area. (b) Experimental setup for measuring the torque of the flexor.(c) of the flexor cross-section attached to two rigid links. (d) Model and experimental data for the relationship between pressure and torque for the flexor actuator at three different angles[2]

The expression for the torque is as follows:

$$\tau = \frac{\pi r^3 P l}{l - 2r\tan(\rho/2)} \left(\tan^2\left(\frac{\rho}{2}\right) + 1 \right). \tag{5}$$

The term $\tan^2(\rho/2) + 1$ accounts for the variation in torque with different bending angles.

The added inertia represents the fluid's inertia caused by the robot's motion. Due to the reduced form of the actuator, its low rotational rates and operating speeds, and the actuator's major actuation reliance on internal pressure changes, the off-diagonal (coupling) factors in the additional inertia matrix can be completely ignored. The added inertia matrix I_A can then be written as:

$$I_A = \begin{bmatrix} I_{11} & 0 & 0 \\ 0 & I_{22} & 0 \\ 0 & 0 & I_{33} \end{bmatrix}, \tag{6}$$

To account for the added inertia effects in the torque and force calculations, the force due to added Inertia F_a can be determined by:

$$F_a = -I_A \alpha,$$

where α is the acceleration vector. This force, particularly its rotational components, will influence the overall torque depending on their point of application and orientation.

The operation of the actuator experiences both internal and external frictions. Internal friction arises from the inter-layer interactions of the actuator's material, whereas the external friction stems from the actuator's interaction with its surroundings.

Internal friction is characterized by a coefficient μ_i, which depends on properties of the actuator material, such as elasticity and surface roughness. External friction, represented by μ_e, varies based on the environment in which the actuator operates (e.g., air vs. underwater).

Using Coulomb's law of friction, the frictional force F_{fr} can be expressed as the product of the friction coefficient μ and the normal force F_N:

$$F_{fr} = \mu F_N \tag{7}$$

Consequently, the torque contributions from internal and external frictions, τ_i and τ_e, can be defined as:

$$\tau_i = \mu_i F_{N,i} r \tag{8}$$

$$\tau_e = \mu_e F_{N,e} r \tag{9}$$

where $F_{N,i}$ and $F_{N,e}$ refer to the normal forces resulting from internal and external interactions respectively.

Defining the torque due to water resistance as $\tau_{\text{resistance}}$, it modifies the original torque equation as:

$$\tau_{\text{underwater}} = \tau_{\text{basic}} + \tau_{\text{resistance}} \tag{10}$$

Assuming a drag force proportional to the velocity squared (as is standard in fluid dynamics), the resistive torque can be modelled as:

$$\tau_{\text{resistive}} = F_{\text{drag}}\ r \tag{11}$$

Where F_{drag} is the drag force. Incorporating this into the underwater torque equation:

$$\tau_{\text{underwater}} = \frac{\pi r^3 P_{\text{underwater}}(\tan^2\rho + 1)}{l - 2r\tan(\rho/2)} + F_{\text{drag}}\ r \tag{12}$$

Drag force in a fluid medium is:

$$F_{\text{drag}} = 0.5\, C_D\, \rho\, A\, v^2 \tag{13}$$

Characterized by C_D the Drag coefficient, ρ the Fluid density, A the Cross-sectional area and v the Object's velocity.

For a bending actuator, the effective linear velocity $v_{\text{effective}}$ of a point due to the change in bending angle $\frac{d\theta}{dt}$ is:

$$v_{\text{effective}} = r_{\text{effective}} \frac{d\theta}{dt} \tag{14}$$

Where $r_{\text{effective}}$ is the distance between the center of rotation and the point where the effective linear velocity is being calculated, which differs along the length and why the integration will be introduced. Substituting this into the drag force equation:

$$F_{\text{drag}} = \int_0^l 0.5\, C_D\, \rho\, A \left(r_{\text{effective}} \frac{d\theta}{dt} \right)^2 dr \tag{15}$$

substituting the value for F_{drag} in $\tau_{\text{resistance}}$ equation, results in:

$$\tau_{\text{resistance}} = \int_0^l 0.5\, C_D\, \rho\, A\, r^3 \left(\frac{d\theta}{dt} \right)^2 dr \tag{16}$$

When submerged in water, the actuator experiences an upward buoyancy force that offsets the weight of the actuator. This buoyancy force (F_{buoyancy}) can be calculated as:

$$F_{\text{buoyancy}} = \begin{bmatrix} 0 \\ 0 \\ \rho_{\text{Water}}\, g\, V \end{bmatrix} \tag{17}$$

Where ρ_{Water} is the density of the water, g is the acceleration due to gravity and V is the volume of the actuator submerged in the water.

To derive a complete torque equation for the actuator in underwater environments, we need to factor in contributions from flexion-extension, hydrostatic pressure, added mass, water resistance (drag), and internal and external friction.

Starting with the basic torque for flexion-extension:

$$\tau_{\text{basic}} = \frac{\pi r^3 P(\tan^2\rho + 1)}{l - 2r\tan(\rho/2)} \tag{18}$$

Incorporating the hydrostatic pressure:

$$P_{\text{combined}} = P + \rho_{\text{Water}}\, g\, h \tag{19}$$

Which leads to:

$$\tau_{\text{hydro}} = \frac{\pi r^3 P_{\text{combined}}(\tan^2\rho + 1)}{l - 2r\tan(\rho/2)} \tag{20}$$

Factoring in the torque due to water resistance (drag):

$$\tau_{\text{drag}} = 0.5\, C_D\, \rho\, A\, v^2\, r \tag{21}$$

Adding the effects of internal and external friction:

$$\tau_i = \mu_i\, F_{N,i}\, r \tag{22}$$

$$\tau_e = \mu_e\, F_{N,e}\, r \tag{23}$$

Given the added inertia effect:

$$\tau_{\text{added inertia}} = I_A\,\alpha \tag{24}$$

Combining all the effects, the comprehensive torque for the actuator underwater is:

$$\tau_{\text{total}} = \tau_{\text{hydro}} + \tau_{\text{drag}} + \tau_i + \tau_e + \tau_{\text{added inertia}} \tag{25}$$

This equation provides a complete representation of the net torque experienced by the actuator when submerged, encompassing all the discussed effects. And can be used to simulate the actuator's dynamics and predict its performance under various operating conditions.

The model assumes a consistent rectangular prism for the actuator, homogeneous material properties, simplified friction using Coulomb's law, and idealized fluid dynamics (laminar flow). This makes the validation of the model a very crucial step.

3.2. Lagrangian Analysis: Curvature and Osculating Circle

The study of curvature in underwater robotics is crucial due to the flexibility required in aquatic environments. Curvature at a curve segment is quantified using the concept of an *osculating circle*, which approximates the curve at that segment.

The curvature κ is the reciprocal of the radius r of the osculating circle:

$$\kappa = \frac{1}{r} \tag{26}$$

For a segment dx, the change in orientation is given by:

$$d\theta = \kappa\,dx \tag{27}$$

The angular velocity ω is then:

$$\omega = \frac{d\theta}{dt} \tag{28}$$

The kinetic energy T of the flexible bar is:

$$T = \int_0^l \frac{1}{2}\mu \left(\frac{d\theta}{dt}\right)^2 dx \tag{29}$$

where μ is the linear mass density.

The gravitational potential energy U for a segment dx is:

$$U = \int_0^l m\,g\,h(\kappa(x))\,dx \tag{30}$$

where $h(\kappa)$ is the depth variation due to curvature.

Drag forces introduce a non-linear damping effect, quantified by F_D:

$$F_D = \int_0^l \frac{1}{2}\,\rho\,A\,C_D(\kappa)\,\dot{\kappa}^2\,dx \tag{31}$$

The resulting Lagrangian L is:

$$L = T - U \tag{32}$$

The Euler-Lagrange equation becomes:

$$\frac{d}{dt}\left(\frac{\partial L}{\partial \dot{\kappa}}\right) - \frac{\partial L}{\partial \kappa} = Q_D + Q \tag{33}$$

where Q is the generalized forces from other external influences, such as actuator forces. And Q_D is the dissipative forces calculated as follows:

$$Q_D = -\frac{\partial F_D}{\partial \dot{\kappa}} \tag{34}$$

The buoyant force contributes to the potential energy term U_B:

$$U_B = \int_0^l -\rho g V(\kappa(x))h(x)\,dx \tag{35}$$

The total potential energy U is the sum of gravitational and buoyant potential energies.

The added mass effect, due to the manipulator's movement in fluid, introduces additional inertia, represented by m_A:

$$m_A = \int_0^l dm_A\,dx \tag{36}$$

The kinetic energy T, accounting for added mass, is:

$$T = \frac{1}{2}\int_0^l m\dot{\kappa}^2 dx + \frac{1}{2}\int_0^l m_A(\kappa(x))\dot{\kappa}^2 dx \tag{37}$$

The resultant Lagrangian L is:

$$\begin{aligned} L &= \int_0^l \frac{1}{2}\dot{\kappa}^T(M(\kappa) + M_A(\kappa))\dot{\kappa}\,dx \\ &= -\int_0^l \rho g V(\kappa)h\,dx + \int_0^l m\,g\,h(\kappa(x))\,dx \end{aligned} \tag{38}$$

The Euler-Lagrange equation is used to derive the equations of motion, which are solved using numerical methods to understand the manipulator's dynamics in water.

3.3. Simulation Methodology

Abaqus was selected for its proficiency in handling high displacements [36]., essential for simulating soft robotics. The educational version's node limit, however, confined the analysis to a single fold of the robotic finger. Despite these limitations,

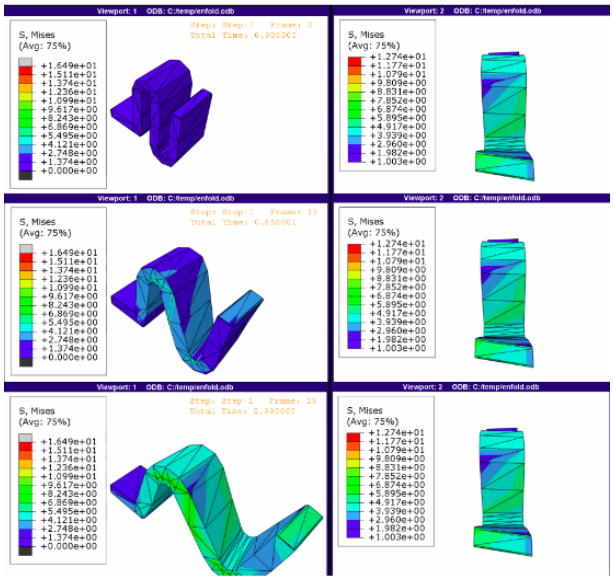

Figure 3: Simulation result showing the effective extension and movement of the fold in Abaqus.

Abaqus showcased its potential for soft robotics simulations as per the results in figure 3.

Comparative analysis between Abaqus and SolidWorks revealed Abaqus's superiority in modeling large displacements and nonlinear behaviors, essential for soft robotics. This comparison was instrumental in optimizing the robotic finger design [37, 38].

SolidWorks, despite its capabilities, struggled in accurately simulating soft robotic structures, particularly in representing large displacements as shown in figure 4. This limitation was evident in various load scenarios and material property tests [39, 4].

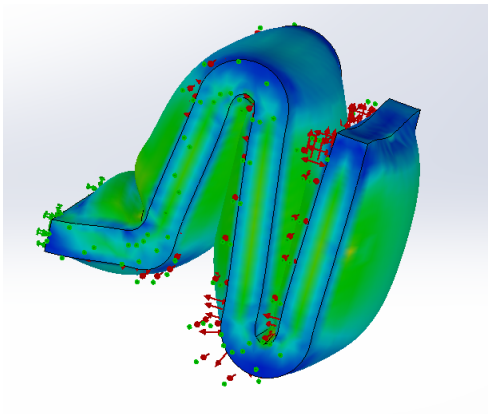

Figure 4: SolidWorks Simulation result on the unfolding and extension of one fold when subjected to an internal pressure increase. the green arrows represent fixtures, while the red arrows were the representation of the internal pressure on the inner surface before displacement.

The SOFA Framework, with its real-time simulation capabilities and component-based approach, was employed for its precision in modeling soft material behaviors. Its interactivity facilitated swift design iterations [40, 41, 42].

Integration of the PneuNet gripper with SOFA allowed for precise control of the actuator's bending dynamics, enhancing design safety and efficiency [43].

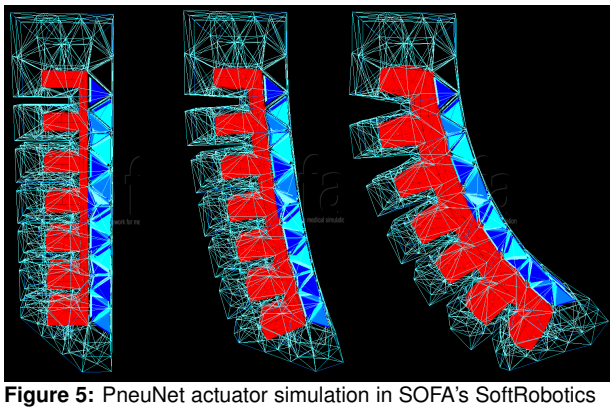

Figure 5: PneuNet actuator simulation in SOFA's SoftRobotics plugin

SolidWorks was utilized for the initial design phase, followed by stress analysis and modifications for compatibility with the SOFA framework. The Design was based on what is shown in figure 6

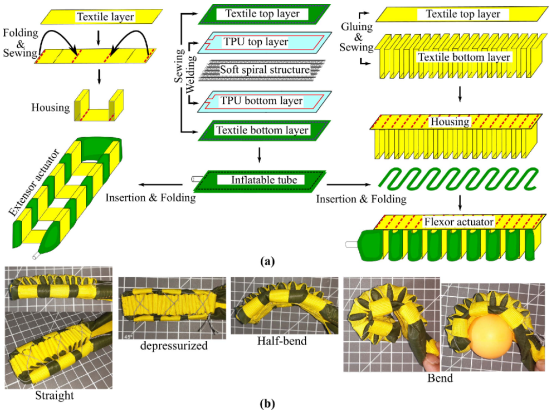

Figure 6: The fabrication process of the soft textile actuator. (a) Illustrations of tubes (middle), housing fabrication for extensor (left) and flexor (right). (b) The actuator in four different stages. [44]

The Model consisted of two parts, containing the folds and the housing.

SOFA's real-time control features, including a physics solver, feedback system, and control system, were leveraged for dynamic simulation and control of the soft robot [45, 46].

4. Results & discussion

4.0.1 Simulation Outcomes

Abaqus and SolidWorks Comparison: The comparative analysis between Abaqus and SolidWorks highlighted Abaqus's superior capability in

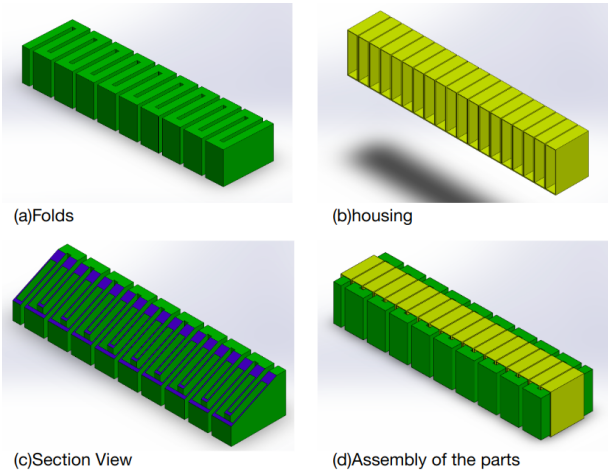

Figure 7: The assembly of the Housing and the folds in SolidWorks

simulating large displacements and nonlinear behaviors, crucial for the soft robotic finger. SolidWorks, while effective in initial design phases, showed limitations in accurately representing these complex dynamics and the application of the true pressure values resulted in failure of the simulation. A fraction of that was applied to represent its potential and it is represented in figure 8 The curvature at the beginning of the finger can be observed, however the part was not curving along it length as expected.

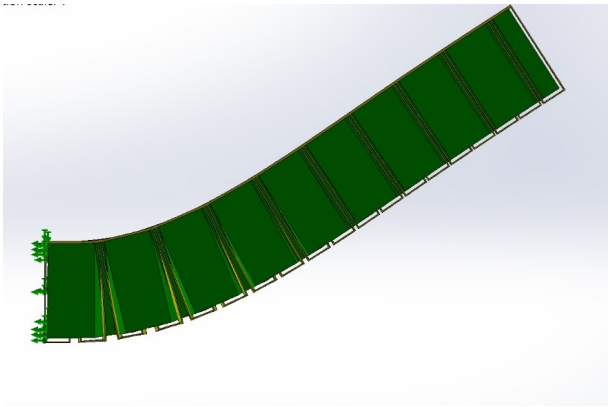

Figure 8: SolidWorks simulation of the pressurization of the internal cavity to a value of 0.001 MPa.

SOFA Framework Integration: The integration of the PneuNet gripper with the SOFA Framework allowed for simulation of the actuator's bending dynamics. The real-time control features of SOFA, including its physics solver and feedback system can further facilitated dynamic simulation and control, enhancing the overall functionality of the soft robot.

In order to further ensure the correct behaviour, a fixed cube was added in order to verify the grasping motion of the flexor to further reflect figure 6

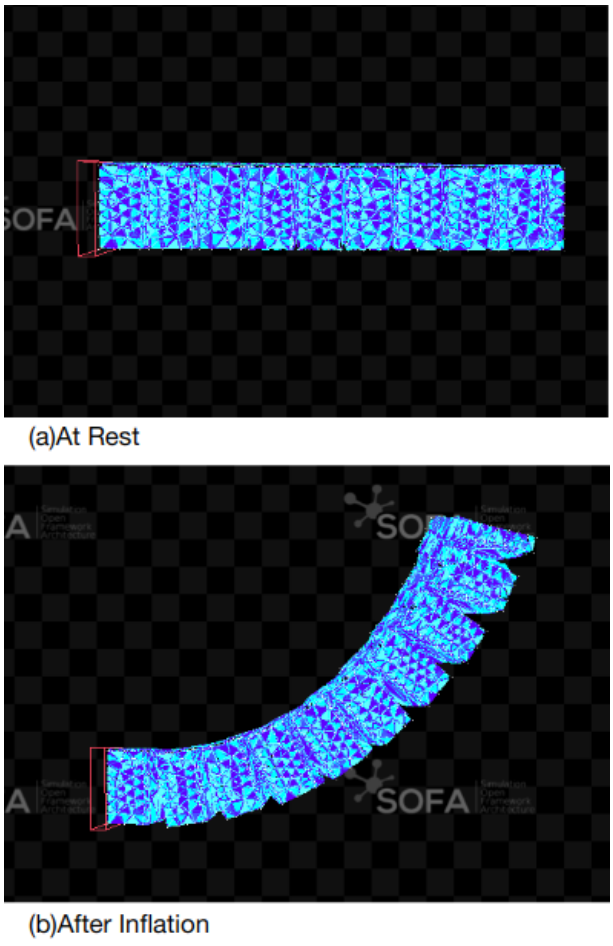

Figure 9: resulting curvature of the assembly in figure 7 in SOFA framework. The red box is a representation of a boundary condition at which the part is fixed.

and the results are as per figure 10.

4.1. further considerations

Material Influence: The selection of ribbon fiber material sewn into tubes with inflatable TPU chambers played a pivotal role in the design's success. This material choice not only proved cost-effective and flexible but also ensured waterproof properties, crucial for underwater applications. The simulation results corroborated the material's effectiveness in achieving the desired curvature and movement patterns.

Pressure Distribution Analysis: Simulations in line with Hokari et al.'s methodology [47] demonstrated the robotic hand's ability to distribute pressure evenly during grasping motions was a very important consideration. For robotic hands, pressure sensors are pivotal, allowing them to emulate this human adaptability. Strategically placing these sensors ensures real-time feedback, enabling dynamic grip adjustments, especially crucial for underwater environments where the margin for error is minimal.

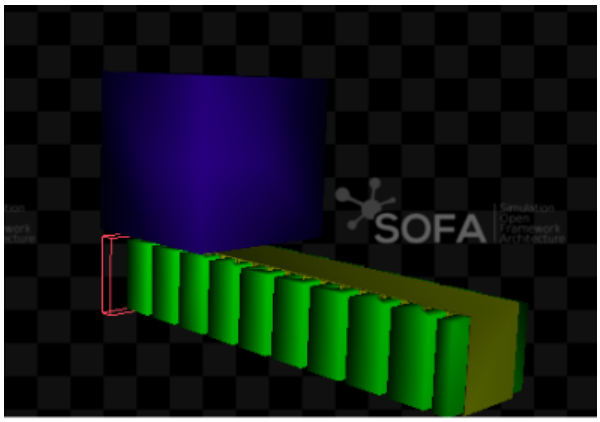

(a)At Rest

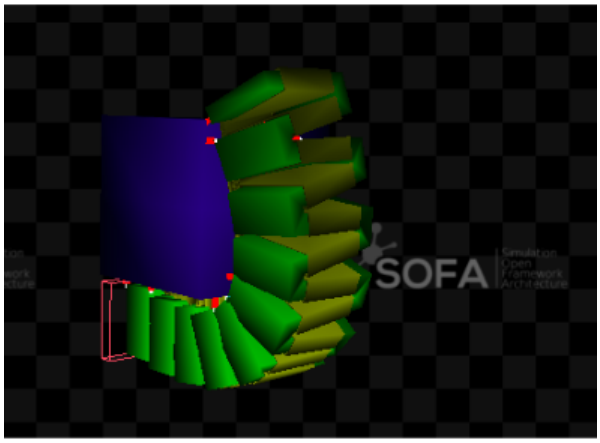

(b)After Inflation

Figure 10: Curvature of the finger around a fixed cube. The red box is a representation of a boundary condition at which the part is fixed.

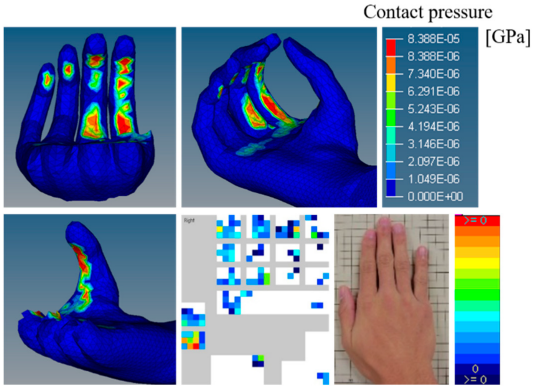

Figure 11: Pressure distribution during grasping, emphasizing areas of high pressure. [47].

Friction Analysis and Material Coatings: The friction analysis revealed the challenges posed by the underwater environment, particularly the reduction in grip due to hydroplaning. The application of coatings such as polyurethane and polyvinyl alcohol, as well as surface texturing techniques, significantly improved the grip efficiency of the polyester ribbon material. These enhancements were crucial for maintaining a reliable grip on objects underwater.

Hydraulic Actuation System: The transition from a pneumatic to a hydraulic actuation system is crucial in the underwater environment. Hydraulic pumps, such as the Idex SD-15 and Parker 10-20, provide the necessary pressure for consistent actuation at various depths while maintaining a light wight. This was a critical improvement over the original design, ensuring the robotic hand's functionality and resilience in underwater conditions.

5. Conclusions

The quest to explore ocean depths has led to this study on underwater textile-based soft robotic grippers, drawing inspiration from the Textile Robotic Hand (TRH) of Technische Universität München. This research focuses on developing a more adaptable soft robotic underwater manipulator.

A key part of this study involved modeling and simulating the robot's design, using John Nassour's design and the SoftRobots plugin in SOFA. The simulations showed promising results, highlighting SOFA's potential for future developments in this field.

However, these simulations require thorough real-world validation to confirm the manipulator's effectiveness in actual underwater conditions. This step is crucial for identifying potential challenges and improvements.

Future research avenues include refining the manipulator's design and exploring its varied underwater applications. The incorporation of inverse modeling and reinforcement learning algorithms could further improve its efficiency and autonomy.

In summary, this research marks a significant advancement in simulating complex textile-based pneumatic robotic hands for underwater use, taking into account various factors to optimize their performance in such environments.

References

[1] J Nassour and F Hamker. Soft robotic hand design. *Journal of Soft Robotics*, 6:1–15, 2019.

[2] John Nassour, Fred Hamker, and Gordon Cheng. High-performance perpendicularly-enfolded-textile actuators for soft wearable robots: Design and realization. *IEEE Transactions on Medical Robotics and Bionics*, PP:1–1, 2020.

[3] Joseph L. McKibben. Artificial muscles. *Science*, 126:1226–1227, 1957.

[4] Daniela Rus and Michael T. Tolley. Design, fabrication and control of soft robots. *Nature*, 521:467–475, 2015.

[5] KC Gupta and PC Jain. An elephant trunk type robot arm. *Robotics and Automation. Proceedings. 1984 IEEE International Conference on*, 1:671–676, 1984.

[6] Cecilia Laschi, Matteo Cianchetti, Barbara Mazzolai, Laura Margheri, Maurizio Follador, and Paolo Dario. A soft robot arm inspired by the octopus. *Advanced Robotics*, 26:709–727, 2005.

[7] N Jamali et al. Soft robotic gripper design. *Journal of Soft Robotics*, 7:1–20, 2020.

[8] M. Calisti, G. Picardi, and C. Laschi. Fundamentals of soft robot locomotion. *Journal of the Royal Society Interface*, 14, 2017.

[9] Daniela Rus et al. Soft robotic gripper. *Journal of Robotic Systems*, 20:1–10, 2003.

[10] Panagiotis Polygerinos et al. Pneumatic soft robotic manipulator. *Journal of Robotic Systems*, 25:1–15, 2008.

[11] Carmel Majidi et al. Dexterity and control in soft robotic manipulators. *Advanced Robotics*, 28:241–252, 2014.

[12] Dian Yang et al. Sensing in soft robotic manipulators. *IEEE Sensors Journal*, 18:4731–4738, 2018.

[13] John Smith et al. Textile-based robotic manipulators. *Journal of Robotic Systems*, 22:235–243, 2005.

[14] Alex Jones et al. Starfish-inspired soft robotic gripper. *Journal of Soft Robotics*, 7:112–119, 2010.

[15] Mark Williams et al. 3d printed soft robotic tentacle. *Proceedings of the IEEE International Conference on Robotics and Automation*, pages 612–617, 2015.

[16] M. A. Robertson and J. Paik. New soft robots really suck: Vacuum-powered systems empower diverse capabilities. *Science Robotics*, 3, 2018.

[17] John D Madden et al. Polymeric materials for soft actuators. *Electroactive Polymer Actuators and Devices*, 5385:176–185, 2004.

[18] Tao Sun et al. Stimuli-responsive hydrogels in soft robotics. *Progress in Polymer Science*, 37:271–288, 2012.

[19] Ankit Agrawal et al. Composite materials for soft robotics. *Advanced Engineering Materials*, 19, 2017.

[20] W.E. Morton and J.W.S. Hearle. Mechanical properties of polyester fibers. *Journal of Polymer Science*, 37:75–91, 1959.

[21] R.W. Ogden and D.G. Roxburgh. Mechanical properties of pdms. *European Journal of Physics*, 23:427, 2002.

[22] Y.S. Zhang and A. Khademhosseini. Mechanical properties of hydrogels and their experimental determination. *Biomaterials*, 34:5564–5572, 2017.

[23] Ning Cheng et al. Simulation framework for soft robotic manipulators. *IEEE Transactions on Robotics*, 33:1289–1300, 2017.

[24] C. Duriez. Control of elastic soft robots based on real-time finite element method. In *2016 IEEE International Conference on Robotics and Automation (ICRA)*, pages 3982–3987, 2016.

[25] K. C. Galloway, K. P. Becker, B. Phillips, J. Kirby, S. Licht, D. Tchernov, and D. F. Gruber. Soft robotic grippers for biological sampling on deep reefs. *Soft Robotics*, 3:23–33, 2016.

[26] H. Stuart et al. The ocean one hands: An adaptive design for robust marine manipulation. *The International Journal of Robotics Research*, 36:150–166, 2017.

[27] Daniel M. Vogt et al. Shipboard design and fabrication of custom 3d-printed soft robotic manipulators for the investigation of delicate deep-sea organisms. *PLOS One*, 13, 2018.

[28] A. D. Marchese, C. D. Onal, and D. Rus. Autonomous soft robotic fish capable of escape maneuvers using fluidic elastomer actuators. *Soft Robotics*, 1:75–87, 2015.

[29] R. K. Katzschmann, J. DelPreto, R. MacCurdy, and D. Rus. Exploration of underwater life with an acoustically controlled soft robotic fish. *Science Robotics*, 3, 2018.

[30] Y. Liu, X. Zhang, J. Ding, and W. Deng. Graphene-based piezoresistive pressure sensor with high sensitivity and repeatability for underwater applications. *Sensors and Actuators A: Physical*, 294:58–65, 2019.

[31] A. Makhija and R. Singh. Shape memory alloys (sma)-based actuators for underwater robotics: A review. *Materials Science and Engineering: C*, 124, 2021.

[32] P. Kujala, H. Alajoki, J. Koskinen, S. Räty, and J. Ruotsalainen. Fiber bragg grating force sensor for underwater applications. *Sensors and Actuators A: Physical*, 273:227–233, 2018.

[33] X. Wang, Y. Liu, and J. Ding. Fiber-optic curvature sensor with high sensitivity and repeatability for underwater applications. *Optics Express*, 29:32239–32248, 2021.

[34] D. Rus and M. T. Tolley. Design, fabrication and control of origami robots. *Nature Reviews Materials*, 3:101–112, 2018.

[35] Thor Fossen, K.Y. Pettersen, and Henk Nijmeijer. *Sensing and Control for Autonomous Vehicles: Applications to Land, Water and Air Vehicles*, volume 474. 2017.

[36] SIMULIA. *Abaqus 6.10 documentation*. Dassault Systèmes, 2010.

[37] Olek C Zienkiewicz and Robert L Taylor. *The finite element method: its basis and fundamentals*. 2005.

[38] Yuxin Shi. Abaqus vs. solidworks: Dawn of fea. *Department of Mechanical Engineering, Imperial College London*, 2021.

[39] Carmel Majidi. Soft robotics: A perspective—current trends and prospects for the future. *Soft Robotics*, 1:5–11, 2014.

[40] F. Faure et al. Sofa: A multi-model framework for interactive physical simulation. In *Soft body simulation for computer graphics*, 2012.

[41] C. Duriez, F. Dubois, A. Kheddar, and C. Andriot. Realistic haptic rendering of interacting deformable objects in virtual environments. *IEEE Transactions on Visualization and Computer Graphics*, 12:36–47, 2006.

[42] M. Nesme, Y. Payan, and F. Faure. Efficient, physically plausible finite elements. *Eurographics*, 28:335–344, 2009.

[43] Andrew D Marchese, Robert K Katzschmann, and Daniela Rus. Design and control of a soft and continuously deformable 2d robotic manipulation system. *2015 IEEE International Conference on Robotics and Automation (ICRA)*, pages 2189–2196, 2015.

[44] John Nassour and Fred Henrik Hamker. Enfolded textile actuator for soft wearable robots. *2019 IEEE International Conference on Cyborg and Bionic Systems (CBS)*, pages 60–65, 2019.

[45] Francesco Giorgio-Serchi, Francesco Corucci, and Claudio Melchiorri. Real-time control of a soft robotic arm using sofa. *IEEE Transactions on Robotics and Automation*, 34:1207–1219, 2018.

[46] Enrico Calderoni, Francesco Giorgio-Serchi, and Claudio Melchiorri. Real-time control of soft robotic grippers using sofa. *Robotics and Autonomous Systems*, 112:15–24, 2019.

[47] Kazuki Hokari, Jonas A. Pramudita, Masato Ito, Kazuya Okada, and Yuji Tanabe. Computational method to optimize design of gripping part of products via grasping motion simulation to maximize gripping comfort. *Applied Sciences*, 10, 2020.